Important Notice to Authors

Attached is a PDF proof of your forthcoming article in Optics Letters. The article Manuscript ID is 471516. *No further processing of your paper will occur until we receive your response to this proof.*

Note: *Excessive proof corrections submitted by the author can result in significant delays to publication. Please include only essential changes that might be needed to address any shortcomings noticed in the proof-preparation process.*

Author Queries

Please answer these queries by marking the required corrections at the appropriate point in the text or referring to the relevant line number in your PDF proof.

Q1	Please provide a definition of DOC at the first mention the text.
Q2	Reference18 is listed in the reference list but not cited in the text. Please cite in the text, else delete from the list.
Q3	The funding information for this article has been generated using the information you provided to us at the time of article submission. Please check it carefully. If any information needs to be corrected or added, please provide the full name of the funding organization/institution as provided in the Crossref Open Funder Registry (https://search.crossref.org/funding).

Other Items to Check

- Please note that the original manuscript has been converted to XML prior to the creation of the PDF proof, as described above. The PDF proof was generated using LaTeX for typesetting. The placement of your figures and tables may not be identical to your original paper.
- Please carefully check all key elements of the paper, particularly the equations and tabular data.
- Author list: Please make sure all authors are presented, in the appropriate order, and that all names are spelled correctly.
- If figures need to be replaced because of accuracy or clarity concerns, please upload each revised figure as an individual PDF at the desired final size. In your corrections, please describe briefly what in the figure(s) has been changed.

Optics Letters

Cylindrical partially coherent scalar sources

R. Martínez-Herrero,[1] O. Korotkova,[2,*] M. Santarsiero,[3] G. Piquero,[1] J. C. G. De Sande,[4] A. V. Failla,[5] and F. Gori[3]

[1] Departamento de Óptica, Universidad Complutense de Madrid, Ciudad Universitaria, 28040 Madrid, Spain
[2] Department of Physics, University of Miami, 1320 Campo Sano Drive, Coral Gables, Florida, 33146, USA
[3] Dipartimento di Ingegneria Industriale, Elettronica e Meccanica, Universitá Roma Tre, Via V. Volterra 62, 00146 Rome, Italy
[4] ETSIS de Telecomunicación, Universidad Politécnica de Madrid, Campus Sur 28031 Madrid, Spain
[5] UKE Microscopy Imaging Facility (UMIF), University Medical Center Hamburg-Eppendorf, 20246 Hamburg, Germany
*Corresponding author: korotkova@physics.miami.edu

Received 25 July 2022; revised 14 September 2022; accepted 15 September 2022; posted 15 September 2022; published 00 xxxxxx 0000

Partially coherent scalar sources with cylindrical symmetry radiating outwards are introduced. Homogeneous cross-spectral densities are shown to possess angularly modulated Hankel modes, whose amplitudes are subject to a filtering process during propagation. Simple criteria for treating such sources are given. For the case of an incoherent cylinder, the number of effective modes is found and spatial coherence is shown to appear in the radiated light. The radial coherence of the radiated field is then examined. Non-homogeneous cylindrical sources are also introduced.

https://doi.org/10.1364/OL.471516

The vast majority of studies on classical coherence deal with radiation from planar sources [1–3]. A notable exception are spherical Schell sources [4–6] being important for the modeling of sunlight coherence [7,8]. Among other curved source models [9], cylindrical structures can be treated with simple mathematical tools. In this connection, we note that the scattering problem of stationary light from a cylinder was solved in Ref. [10], in which it was clearly illustrated that the scattered spectral density's angular distribution cannot be controlled at will and generally assumes a highly oscillatory profile.

In this Letter, we analyze a scalar cylindrical source endowed with partial coherence. To this aim, denoting by a the cylinder radius and using cylindrical coordinates z, r, and φ, we assume the cylinder to be of infinite extent along z, radiating at wavenumber k. The emitted field is assumed to be independent from z. The electric field in the space external to the cylinder can then be expressed as a function of r and φ only, say $E(r, \varphi)$. According to [11], the outgoing radiated field can be expanded into series:

$$E(r, \varphi) = \sum_{n=-\infty}^{\infty} b_n\, H_n(kr)\, e^{in\varphi}; \quad (r \geq a), \tag{1}$$

with a suitable set of b_n coefficients, where H_n denotes an outgoing Hankel function [12], generally written as $H_n^{(1)}$ to distinguish it from the inward going function $H_n^{(2)}$, which we will not use. We stress that, although we consider here scalar cylindrical sources, the same formalism could be used to study vectorial sources when the electric field vector is parallel to the axis.

It will be useful to write the coefficients b_n in the form $c_n/H_n(ka)$. Equation (1) then becomes

$$E(r, \varphi) = \sum_{n=-\infty}^{\infty} c_n \frac{H_n(kr)}{H_n(ka)}\, e^{in\varphi}; \quad (r \geq a), \tag{2}$$

so that across the source surface ($r = a$), the field reduces to

$$E(a, \varphi) = \sum_{n=-\infty}^{\infty} c_n\, e^{in\varphi}. \tag{3}$$

The c_n coefficients can be evaluated by the usual Fourier series rule if the values of E across the source surface are given.

Let us now pass to the partially coherent case where we shall make use of the cross-spectral density (CSD) [3], which in the space external to the source can be written as

$$W(r_1, \varphi_1; r_2, \varphi_2) = \sum_{n=-\infty}^{\infty} \sum_{m=-\infty}^{\infty} \langle c_n^* c_m \rangle \frac{H_n^*(kr_1) H_m(kr_2)}{H_n^*(ka) H_m(ka)} \tag{4}$$

$$\times\; e^{i(m\varphi_2 - n\varphi_1)}; \quad (r_1, r_2 \geq a), \tag{5}$$

where the coefficients c_n become random variables. Here, the asterisk stands for complex conjugate and the angle brackets denote an ensemble average. The CSD in the form of Eq. (5) is well known in optics as the coherent mode decomposition, since [13] (see also [2]). Let us consider, in particular, the CSD across the source surface, which is given by expression:

$$W(a, \varphi_1; a, \varphi_2) = \sum_{n=-\infty}^{\infty} \sum_{m=-\infty}^{\infty} \langle c_n^* c_m \rangle\, e^{i(m\varphi_2 - n\varphi_1)}. \tag{6}$$

Before examining a specific example, let us discuss the effects of propagation upon the Hankel functions [12,14]. First we recall that the moduli of such functions decrease upon propagation, roughly speaking, as cylindrical waves of the form $1/\sqrt{kr}$. We shall call the curve of the decrease of this type the reference curve. This is shown in Fig. 1(a), where the moduli of some Hankel functions at a radius p times a (with $p \geq 1$) divided by the same function at radius a are shown for a few values of n as functions of p, assuming $ka = 100$. This figure permits to see the decrease of $|H_n(pka)/H_n(ka)|$ for increasing p and to compare the decrease rate to the reference curve (black solid curve). All

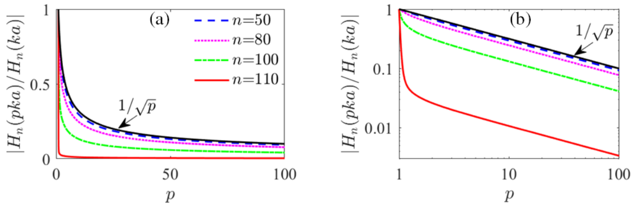

Fig. 1. (a) Ratio $|H_n(pka)/H_n(ka)|$ versus p for $ka = 100$ and several values of n. The black curve is the plot of $1/\sqrt{p}$. (b) Same as in panel (a) but on a log–log scale.

the curves tend to become lines with slope $-1/2$ on a log–log scale, as can be seen in Fig. 1(b).

The key parameter is given by ka. In fact, when n is small enough, as compared to ka, the decrease of $|H_n|$ follows the reference curve (in Fig. 1, where for $ka = 100$, the curves pertaining to $n<30$ are indistinguishable from the reference curve). In contrast, when n is comparable to or greater than ka, a sharp decrease is observed for small values of p, while it presents the same slope as that of the reference curve for longer distances.

To better account for the role of the parameter ka, note that it expresses the ratio between the length $2\pi a$ of the circle limiting the cylinder and the wavelength λ. Since the typical Hankel function H_n is accompanied by the angular Fourier component $\exp(in\varphi)$, when n exceeds ka, the involved phase spatial details are smaller than the wavelength. In a similar problem treated with plane waves, this would involve evanescent waves, which are known to suffer a drastic decrease of amplitude with propagation distance [3]. The same type of behavior is exhibited by Hankel functions. As we shall now see, this qualitative hint is supported by numerical data.

In Fig. 2, the curves $p|H_n(p\,ka)/H_n(ka)|^2$ are drawn as functions of n for a few values of the normalized radial coordinate p. Although n takes integer values, continuous curves have been represented to make their visibility easier. Note that since we deal with functions that are even with respect to n, the plots could be drawn on the negative semiaxis too, making all the curves symmetric with respect to the vertical axis. The lowest curve is the circle arc to be seen in Eq. (7). In Fig. 2(a), a value of 100 is assumed for the parameter ka. It is seen that the main transition from high to low values occurs in a certain interval around $n = ka$. The drop to small values when n exceeds ka becomes increasingly faster on increasing ka. This can be seen in Fig. 2(b), where ka has been raised to 1000. This behavior is accounted for by an asymptotic formula obeyed by Hankel functions, which reads [see Eq. (11) of [15] with $M = 1$]

$$\frac{p|H_n(p\,ka)|^2}{|H_n(ka)|^2} \simeq \sqrt{1-\left(\frac{n}{ka}\right)^2}\ \ \mathrm{step}(ka-|n|), \tag{7}$$

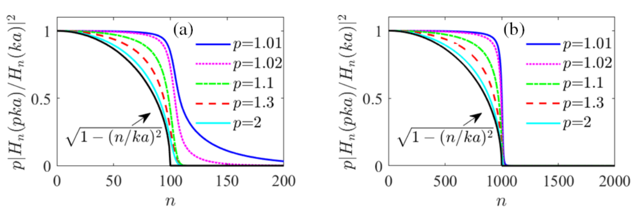

Fig. 2. (a) Ratio $p|H_n(p\,ka)/H_n(ka)|^2$ versus n (treated as a continuous variable) for $ka = 100$ and several values of p. The arc of circle $\sqrt{1-(n/ka)^2}$ is the limiting curve for large ka and for p of the order of a few units. The drawing interval is from 0 to 2 ka. (b) Same as in panel (a) but with $ka = 1000$.

for $p>1$ and $ka \gg 1$, where step denotes the Heaviside unit function [14]. For high enough p and ka, Eq. (7) provides a very good approximation. This is an important point. It shows that no matter how fine details are present on the source surface, only details greater than the wavelength contribute significantly to the propagated field when ka is large enough. Accordingly, the number of effective modes can be taken as $2ka + 1$, and the series of Hankel functions can be well approximated by finite sums.

We shall now examine the main features of CSDs pertaining to fields emitted by cylindrical sources. The simplest category of such CSDs is specified by the following hypothesis:

$$\langle c_n^* c_m\rangle = \delta_{nm}\langle|c_n|^2\rangle \quad \forall n, \tag{8}$$

where δ_{nm} denotes the Kronecker symbol (1 if $n = m$, 0 if $n \neq m$). In this case, Eq. (6) of the CSD across the cylinder surface becomes shift-invariant, i.e., it only depends on the angular distance between the considered points $\Delta\varphi = \varphi_2 - \varphi_1$. More precisely, it reduces to a single Fourier series:

$$W_a(\Delta\varphi) = W(a,\varphi_1;a,\varphi_2) = \sum_{n=-\infty}^{\infty}\langle|c_n|^2\rangle\, e^{in\Delta\varphi}\ ; \tag{9}$$

whose structure as a function of $\Delta\varphi$ depends on the $\langle|c_n|^2\rangle$ parameters. In particular, the spectral density $W(a,\varphi;a,\varphi) = W_a(0)$ is seen to be uniform.

Conversely, a given shift-invariant CSD across the surface will determine the Fourier coefficients as

$$\langle|c_n|^2\rangle = \frac{1}{2\pi}\int_{-\pi}^{\pi} W_a(\psi)e^{-in\psi}\,\mathrm{d}\psi \quad \forall n\ . \tag{10}$$

As is well known, the Bochner theorem [17] requires that for a bona fide shift-invariant, periodic CSD, all the Fourier coefficients are nonnegative. Indeed, this is also requested by the derivation we used, where such coefficients equal the expected values of the random quantities $|c_n|^2$.

According to Eq. (5), the CSD corresponding to the hypothesis of Eq. (8) in the space region external to the source becomes

$$W(r_1,\varphi_1;r_2,\varphi_2) = \sum_{n=-\infty}^{\infty}\langle|c_n|^2\rangle\frac{H_n^*(kr_1)H_n(kr_2)}{|H_n(ka)|^2}\, e^{in\Delta\varphi}\ , \tag{11}$$

with $r_1, r_2 \geq a$. Notice that Eq. (11) has the meaning of a modal expansion [3] whose modes are the Hankel functions multiplied by the Fourier exponentials. The right-hand side of such an equation provides the series to be used to evaluate the CSD for any pair of points whose coordinates appear on the left-hand side as arguments. For brevity, the ratios containing the Hankel functions in Eq. (11) will be called Hankel factors.

Let us now refer to points on the source surface. For what we are going to show, it is convenient to give an approximated expression for the CSD across the surface [Eq. (9)], which can be used whenever the latter is significantly different from zero only for $\Delta\varphi \ll 2\pi$. In such a case, the number of significant terms in the sum is very high and the sum can be approximated by an integral, after considering n as a continuous variable. Therefore,

$$W_a(\Delta\varphi) \simeq \int_{-\infty}^{\infty}\langle|c_n|^2\rangle\, e^{in\Delta\varphi}\,\mathrm{d}n\ , \tag{12}$$

and the CSD reduces to the (inverse) Fourier transform of the function $\langle|c_n|^2\rangle$ evaluated at $\Delta\varphi/(2\pi)$.

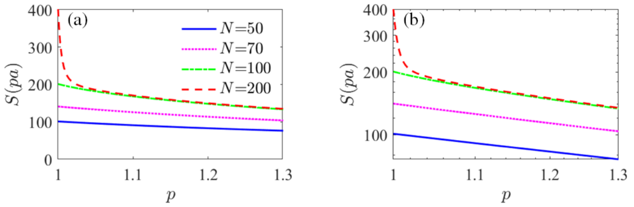

Fig. 3. Spectral density $S(r) = S(pa)$ versus p plotted from Eq. (15) for $A = 1$, $ka = 100$, and several N on a (a) linear and (b) log–log scale.

One of the easiest cases to be considered is when all expansion coefficients are equal to one and the same constant, say A, if $|n|$ does not exceed a given value N and vanishes otherwise, i.e.,

$$\langle |c_n|^2 \rangle = A \quad (|n| \le N); \qquad \langle |c_n|^2 \rangle = 0 \quad (|n| > N). \tag{13}$$

If $N \gg 1$, Eq. (12) can be used by letting $\langle |c_n|^2 \rangle = \mathrm{rect}[n/(2N)]$, so that the CSD turns out to be

$$W_a(\Delta\varphi) = 2NA \,\mathrm{sinc}\,(N\Delta\varphi/\pi)\ , \tag{14}$$

with $\mathrm{sinc}(t) = \sin(\pi t)/(\pi t)$. It becomes increasingly narrower on increasing N and in the limit $N \to \infty$, becomes proportional to the Dirac delta function $\delta(\Delta\varphi)$, which specifies a spatially incoherent source in the azimuthal coordinate.

Let us now consider the effects of propagation. To this aim, we use Eqs. (11) and (13), and first set $r_1 = r_2 = r$, $\varphi_1 = \varphi_2 = \varphi$. Then the spectral density becomes

$$S(r) = W(r, \varphi; r, \varphi) = A \sum_{n=-N}^{N} \frac{|H_n(kr)|^2}{|H_n(ka)|^2}\ , \tag{15}$$

which is apparently angle-independent. The effect of changing the value of N is shown in Fig. 3(a), where $S(r)$ is plotted as a function of p for $ka = 100$ and different values of N. The spectral density across the cylinder surface ($p = 1$) increases linearly on increasing N. The propagated spectral density increases with N too, but only up to $N \approx ka$. After this value, it does not increase any longer, except at very short distances from the surface ($p \lesssim 1.05$). Such a behavior denotes that modes with $N>ka$ do not propagate and remain confined near the cylinder surface. The same quantity is shown in Fig. 3(b), but on a log–log plot: a sharp decrease is observed near the cylinder for $N>ka$, followed by a linear decrease. The negative slope of these lines reflects the cylindrical-like decrease of the spectral density for large enough values of r.

Let us now consider a spatially incoherent source and explore the angular dependence by fixing $r_1 = r_2 = r$. With $N \to \infty$, the CSD in Eq. (11), say W_r, takes on the expression

$$W_r(\Delta\varphi) = W(r, \varphi_1; r, \varphi_2) = A \sum_{n=-\infty}^{\infty} \frac{|H_n(kr)|^2}{|H_n(ka)|^2}\, e^{in\Delta\varphi}. \tag{16}$$

For $r = a$, an infinite number of modes contribute with equal powers. Upon propagation, the Hankel factors become smaller and even negligible for $|n|>ka$. The resulting CSD is affected by a sort of low-pass filtering process illustrated by Fig. 2, which shows how Fourier coefficients (Hankel factors) of the series in Eq. (16) are altered by propagation. Consider Fig. 2(a), let us pass from the highest curve, corresponding to $p = 1.01$, to the lowest one, $p = 2$. This means moving away from the source surface passing from a distance of $0.01a$ to an a value. Concurrently, the curves of the Hankel factors change from a roughly rectangular shape with base $2ka$ to a nearly circular shape with the same base, as predicted by Eq. (7).

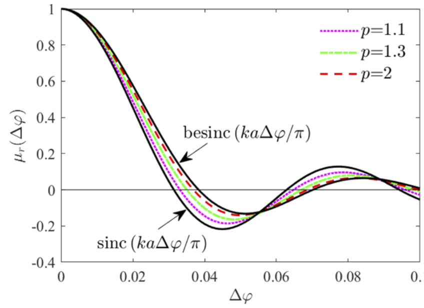

Fig. 4. Degree of coherence μ versus $\Delta\varphi = \varphi_2 - \varphi_1$ (in radians), corresponding to the CSD of Eq. (16) for $ka = 100$ and several values of p, together with the plots of besinc$(ka\,\Delta\varphi/\pi)$ of Eq. (17) and sinc$(ka\,\Delta\varphi/\pi)$.

Recalling Eq. (12), we deduce that when r increases and the curves of Figs. 2(a) and 2(b) pass from a rectangular to a circular shape, the corresponding CSD passes from a sinc to a besinc shape [16], the latter being

$$W_r(\Delta\varphi) \simeq \frac{A}{r}\ \mathrm{besinc}\left(\frac{ka\,\Delta\varphi}{\pi}\right) = \frac{2A}{r}\ \frac{J_1(ka\,\Delta\varphi)}{ka\,\Delta\varphi}, \tag{17}$$

which represents the asymptotic form of the CSD pertaining to the far zone. According to general results [21], the far-zone condition is much less severe than in the coherent case. In fact, it is reached already when r is greater than a few times a.

The same behavior pertains to the angular DOC, defined as Q1

$$\mu_r(\Delta\varphi) = W_r(\Delta\varphi)/W_r(0), \tag{18}$$

which is shown in Fig. 4. Note that, due to symmetry of weights, the DOC is even and real-valued.

For completeness, we add that if the distance $r - a$ becomes smaller than the lowest value ($0.01a$) used in Fig. 2, the DOC curve keeps getting increasingly thinner.

Let us now hint at radial coherence, i.e., to the CSD for two points located at r_1 and r_2 along a given radius ($\varphi_1 = \varphi_2$) as expressed by [see Eq. (16)]

$$W(r_1, \varphi; r_2, \varphi) = \sum_{n=-\infty}^{\infty} \frac{H_n^*(kr_1)H_n(kr_2)}{|H_n(ka)|^2}, \tag{19}$$

which is indeed independent from φ. This function plays a role similar to the z-coherence for planar sources [6,19,20]. In Fig. 5, the modulus of the DOC between two points aligned along a radius is drawn for several values of r_1 as a function of r_2. It is seen that when r_1 grows, the asymptotic value of the DOC for $kr_2 \to \infty$ gets increasingly higher.

As an example of a partially coherent source, we consider a cylindrical source consisting in only four modes (n =1, 5, 10, and 50, with coefficients 1, 0.5, 0.5, and 0.1, respectively) and show in Fig. 6 the angular DOC of the radiated field at three propagation distances. It is apparent that as light moves away from the source, the lowest modes are preserved while the highest are partially suppressed or even completely filtered.

To consider a non-homogeneous source, we note that if we add to Eq. (8) the hypothesis that c_n and c_{-n} are perfectly correlated,

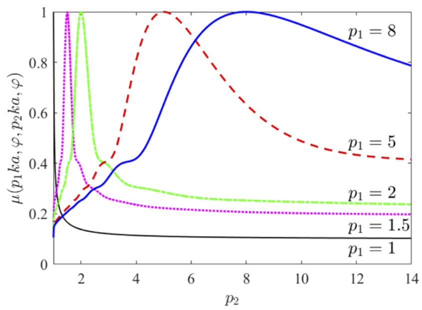

Fig. 5. Modulus of the DOC corresponding to the CSD of Eq. (19) between two points aligned along a radius, at $ka = 100$. Curves are for fixed $p_1 = r_1/a$ versus $p_2 = r_2/a$.

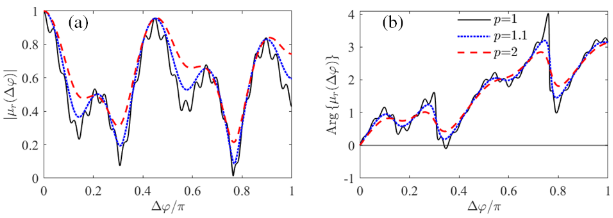

Fig. 6. (a) Modulus and (b) phase of the DOC μ versus $\Delta\varphi$ (radians) of the field radiated by a source with $ka = 10$ and only four modes (n =1, 5, 10, and 50, with coefficients 1, 0.5, 0.5, and 0.1, respectively).

have equal mean squared values, and set $\langle |c_0|^2\rangle = 0$, we arrive at the following family of CSDs:

$$W(r_1, \varphi_1; r_2, \varphi_2) = \sum_{n=1}^{\infty} \langle |c_n|^2\rangle \frac{H_n^*(kr_1) H_n(kr_2)}{|H_n(ka)|^2} \tag{20}$$

$$\times \cos n\varphi_1 \cos n\varphi_2, \tag{21}$$

which is in the form of a new modal expansion, which is seen to be even with respect to both φ_1 and φ_2. In addition, the above CSD is immediately divisible into the sum of a function of $\varphi_1 - \varphi_2$ and of one of $\varphi_1 + \varphi_2$ as follows:

$$W(r_1, \varphi_1; r_2, \varphi_2) = W_-(r_1, \varphi_1; r_2, \varphi_2) + W_+(r_1, \varphi_1; r_2, \varphi_2), \tag{22}$$

$$W_\mp(r_1, \varphi_1; r_2, \varphi_2) = \frac{1}{2} \sum_{n=1}^{\infty} \langle |c_n|^2\rangle \frac{H_n^*(kr_1) H_n(kr_2)}{|H_n(ka)|^2} \tag{23}$$

$$\times \cos n(\varphi_1 \mp \varphi_2). \tag{24}$$

While the first series in Eq. (24) (W_-) depends on $\varphi_1 - \varphi_2$, the second (W_+) depends on $\varphi_1 + \varphi_2$, so that the CSD is no longer angularly shift-invariant. It is also to be noted that the second series alone is not a valid CSD. (For example, a hypothetical CSD $W(\varphi_1, \varphi_2) \propto \cos(\varphi_1 + \varphi_2)$ would predict both positive and negative intensity values.) While not impairing the validity of the overall CSD specified by Eq. (20), these remarks put caveats, once again, on the management of CSDs [22]. As an example, we consider the particular case of a CSD made up of two subsequent modes, say the first two, taken at the same angle. The CSD reads

$$W_2(r_1, \varphi; r_2, \varphi) = \sum_{n=1}^{2} \langle |c_n|^2\rangle \frac{H_n^*(kr_1) H_n(kr_2)}{|H_n(ka)|^2} \cos^2 n\varphi. \tag{25}$$

Letting $\varphi = 0$, we obtain a partially coherent field, while for $\varphi = \pi/4, \pi/2$, we have two completely coherent fields with different radial dependence.

In summary, we saw that cylindrical partially coherent homogeneous sources can be treated with the help of outgoing Hankel functions. This was also derived for some non-homogeneous sources. These cases are added to the few known examples of modal analysis for curved sources. Several examples were developed for which the closed form expressions of the CSDs are obtainable in the far zone.

A possible way to realize the sources under study can be through the use of the radiation coming from a line source lying on the cylinder axis, and nematic crystal light modulators realized on a cylindrical surface, following analogous procedures as those adopted for planar sources. With the new type of sources, an important problem of stationary light fully controllable in 360° is solved which is required for illumination/sensing/communication technologies in biomedical and environmental optics.

Funding. Ministerio de Economía y Competitividad (PID2019-104268 GB-C21). Q3

Disclosures. The authors declare no conflicts of interest.

Data availability. No data were generated or analyzed in the presented research.

REFERENCES

1. J. W. Goodman, *Statistical Optics* (Wiley, 2005).
2. L. Mandel and E. Wolf, *Optical Coherence and Quantum Optics* (Cambridge University Press, 1995).
3. O. Korotkova, *Theoretical Statistical Optics* (World Scientific, 2021).
4. F. Gori and O. Korotkova, Opt. Commun. **282**, 3859 (2009).
5. R. Borghi, F. Gori, O. Korotkova, and M. Santarsiero, Opt. Lett. **37**, 3183 (2012).
6. F. Gori, M. Santarsiero, J. C. G de Sande, G. Piquero, O. Korotkova, A. V. Failla, and R. Martinez-Herrero, "Partially coherent spherical sources with spherical harmonic modes," (submitted to J. Opt. Soc. A).
7. G. S. Agarwal, G. Gbur, and E. Wolf, Opt. Lett. **29**, 459 (2004).
8. S. Divitt and L. Novotny, Optica **2**, 95 (2015).
9. V. H. Schultheiss, Batz, U. Peschel, and S. , Adv. Phys.: X **5**, 1759451 (2020).
10. M. W. Hyde, A. E. Bogle, and M. J. Havrilla, Opt. Express **21**, 32327 (2013).
11. W. K. H. Panofsky and M. Phillips, *Classical Electricity and Magnetism* (Addison-Wesley, 1969).
12. G. J. Gbur, *Mathematical Methods for Optical Physics and Engineering* (Cambridge University Press, 2011).
13. H. Gamo, J. Phys. Soc. Jpn. **19**, 1955 (1964).
14. G. B. Arfken and H. J. Weber, *Mathematical Methods for Physicists, Sixth Edition* (Elsevier, 2005).
15. A. Erdelyi, *Higher Trascendental Functions, Vol. II* (McGraw-Hill, 1953).
16. A. Papoulis, *Systems and Transforms with Applications in Optics* (McGraw-Hill, 1968).
17. F. Riesz and B. Sz.-Nagy, *Functional Analysis* (Ungar, 1955).
18. E. Wolf, *Introduction to the Theory of Coherence and Polarization of Light* (Cambridge, 2007). Q2
19. F. Gori, R. Martínez-Herrero, G. Piquero, J. C. G de Sande, O. Korotkova, and M. Santarsiero, Opt. Lett. **47**, 1681 (2022).
20. O. Korotkova, F. Gori, M. Santarsiero, R. Martínez-Herrero, G. Piquero, and J. C. G de Sande, Opt. Lett. **47**, 2394 (2022).
21. F. Gori, Opt. Lett. **30**, 2840 (2005).
22. F. Gori and R. Martínez-Herrero, J. Opt. Soc. Am. A **38**, 737 (2021).